Liquid Crystals
Publication details, including instructions for authors and subscription information:
http://www.informaworld.com/smpp/title~content=t713926090

Synthesis and properties of 5,10,15,20-tetra[(4-alkoxy-3-ethyloxy)phenyl]porphyrin hydroxylanthanide liquid crystal complexes

Miao Yu[a]; Guofa Liu[a]; Yuchuan Cheng[a]; Weiqing Xu[a]
[a] College of Chemistry, Jilin University, Changchun, China

To cite this Article Yu, Miao , Liu, Guofa , Cheng, Yuchuan and Xu, Weiqing(2005) 'Synthesis and properties of 5,10,15,20-tetra[(4-alkoxy-3-ethyloxy)phenyl]porphyrin hydroxylanthanide liquid crystal complexes', Liquid Crystals, 32: 6, 771 — 780
To link to this Article: DOI: 10.1080/02678290500139591
URL: http://dx.doi.org/10.1080/02678290500139591

Liquid Crystals, Vol. 32, No. 6, June 2005, 771–780

Taylor & Francis
Taylor & Francis Group

Synthesis and properties of 5,10,15,20-tetra[(4-alkoxy-3-ethyloxy)phenyl]porphyrin hydroxylanthanide liquid crystal complexes

MIAO YU, GUOFA LIU*, YUCHUAN CHENG and WEIQING XU
College of Chemistry, Jilin University, Changchun, 130023, China

(*Received 19 November 2004; accepted 6 February 2005*)

Twelve 5, 10, 15, 20-tetra[(4-alkoxy-3-ethyloxy)phenyl]porphyrin hydroxylanthanide complexes Ln[$(C_n$OEOP$)_4$P](OH) (n=12, 14, 16; Ln=Tb, Dy, Er, Yb) and three ligands have been synthesized and their composition, structure and spectral properties studied. Their liquid crystalline behaviour is also presented. Differential scanning calorimetry and polarizing optical microscopy reveal that all exhibit a discotic liquid crystalline phase. X-ray diffraction shows that the mesophase is a hexagonal columnar, Col_h. The lanthanide ion, which is coordinated to the four nitrogen atoms of the porphyrin and to the oxygen atom of the hydroxyl group, is out of the porphyrin molecular plane. All the complexes are stable below 200°C and undergo complete decomposition at 800°C. The fluorescence quantum yields of the lanthanide complexes are much lower than those of the corresponding ligands. The electrochemical studies show that the redox potentials do not change on varying the chain length.

1. Introduction

Following Wong's [1] synthesis of the first lanthanide porphyrin complexes, ErTPP(acac), in 1974, the field of lanthanide porphyrin complexes developed rapidly [2]. They may be used in photo-electronic conversion, for their biomimetic properties, as catalytic materials, as specific nuclear magnetic resonance shift reagents and so on [2]. Liquid crystals [3, 4] represent one of the best known classes of self-organizing materials, and range from, for example, surfactants that can form micelles, monolayers, and membranes, to the rod-like molecules used in liquid crystal (LC) displays [5]. Goodby *et al.* synthesized the first LC semiconductor [6]. Discotic mesomorphic states are also attracting considerable attention with much work focused on studying the relationships between material functions and mesomorphic structures [7].

Porphyrin liquid crystals [8, 9] are of interest for optoelectronic and other device applications due to their synthetic versatility, thermal stability, large π-electron systems, and photochemical properties [10]. However, these studies have focused mainly on porphyrin ligands, or transition metal porphyrin [11]. Trivalant rare earth ions are known for their unique optical properties such as line-like emission bands and relatively long luminescence lifetimes [12]. These unique properties have drawn considerable interest for their potential application. To the best of our knowledge, there have been few studies on a series of lanthanide monoporphyrin liquids using cyclic voltammetry and luminescence spectroscopy. In this paper twelve meso–tetra[(4-alkoxy-3-ethyoxy)phenyl]porphyrin hydroxylanthanide complexes have been synthesized. Their composition, structure and spectral properties have been investigated by elemental analysis, UV-visible spectra, infrared spectra, molar conductances, ^{1}H NMR spectra, luminescence spectra, thermal stability and electrochemistry. Their liquid crystalline properties were studied using differential scanning calorimetry (DSC), polarizing optical microscopy (POM), and X-ray diffraction (XRD).

2. Experimental

2.1. *Apparatus and measurements*

Elemental analysis was performed using a Pekin-Elmer 240C auto elemental analyser. Infrared spectra were recorded on a Nicolet 5PC FTIR spectrometer using KBr pellets in the region 400–4000 cm^{-1}. UV-vis spectra were recorded on a Shimadzu UV-240 spectrophotometer in the range 350–700 nm using chloroform as solvent. Molar conductances of 10^{-3} mol dm^{-3} chloroform solutions at 25°C were measured on a DDX-111A

*Corresponding author. Email: jiaqiu_001@163.com

Liquid Crystals
ISSN 0267-8292 print/ISSN 1366-5855 online © 2005 Taylor & Francis Group Ltd
http://www.tandf.co.uk/journals
DOI: 10.1080/02678290500139591

conductometer. The ^{1}H NMR spectra were recorded in deuterated chloroform using a Varian-Unity 400 NMR spectrometer employing tetramethylsilane as internal reference. DSC was undertaken on a Netesch DSC 204. The optical textures were observed using a XinTian XP1 (CCD: TOTA-500 II) polarized light microscope equipped with a variable temperature stage (Linkam TMS 94). XRD patterns were recorded using a Shimadzu XRD-6000. Excitation and emission spectra at room temperature in the region 300–800 nm using 10^{-5} mol dm^{-3} chloroform solutions were measured using a FS920 steady state fluorescence spectrometer. Redox potentials of the porphyrins in DMF, containing 0.1M TBAP as a supporting electrolyte, at room temperature were determined by cyclic voltammetry using a three-electrode system under deaerated conditions and a CHI 600A electrochemical analyser.

2.2. *Synthesis of the ligands and complexes*

Meso–tetra(4-hydroxy-3-ethyloxy)phenylporphyrin (THEPPH_2) was prepared as described in the literature [13]. Meso-tetra[(4-dodecyloxy-3-ethyloxy)phenyl]porphyrin ligand (TDEPPH_2) was prepared thus: THEPPH_2 and 1-bromododecane were heated under reflux in benzene under the protection dry nitrogen for 3 h. The crude product was purified by column chromatotgraphy on neutral alumina, eluting by chloroform, and recrystallized from chloroform/hexane. Other ligands [(4-tetradecyloxy-3–ethyloxy)phenyl]prophyrin, [(4-hexadecyloxy-3-ethyloxy)phenyl]porphyrin were prepared by a similar method.

Meso-tetra[(4-dodecyloxy-3-ethyloxy)phenyl]porphyrin hydroxy - rare earth complex Er[(C_{14}OEOP)$_4$P(OH)] (C_{14}O=dodecyloxyl; EOP=ethyloxyphenyl; P=porphyrin; Ln=Tb, Dy, Er, Yb) was prepared by the following procedure. The free base H_2[(C_{14}OEOP)$_4$P] (0.30 g) and the hydrate $ErCl_3 \cdot 6H_2O$ (0.60 g) were heated in molten imidazole (10.0 g) at 210°C under the protection and stirring of a dry nitrogen stream for 2 h. The extent of the reaction was monitored by measuring the UV-vis spectra of the reaction solution at 10 min intervals. After cooling to 100°C, 150 ml distilled water was added into the reaction mixture and the solution filtered, washed several times with distilled water in a separating funnel, and finally the product was dried under vacuum.

The crude product was dissolved in 200 ml chloroform. The solution was washed with 100 ml 0.1% aqueous $AgNO_3$ and the chloroform layer separated; 30 ml of chloroform and 20 ml of methanol were added to the separated chloroform. The mixture was again washed with 100 ml 0.1% aqueous $AgNO_3$ several times until no more AgCl precipitated. The chloroform solution was concentrated and chromatographed on a neutral alumina column. The first band containing a small amount of ligand, H_2[(C_{14}OEOP)$_4$P], was eluted with chloroform. The second band containing the target compound was eluted with chloroform containing 20% methanol. The product was obtained by concentration of the solution and drying under vacuum. Other complexes, Ln[(C_nOEOP)$_4$P](OH) (Ln=Yb, Dy, Tb), were prepared by similar methods.

3. Results and disscussion

3.1. *Composition of the complexes*

The reaction of hydrated $LnCl_3 \cdot 6H_2O$ with free ligand porphyrin in imidazole may be described by the equation:

$$H_2\left[(CnOEOP)_4P\right] + LnCl3{\cdot}6H2O \xrightarrow[210^{\circ}C]{\text{imidazole}} Ln\left[(CnOEOP)_4P(OH)\right] + HCI + 5H_2O.$$

The elemental analytical data for carbon, hydrogen, nitrogen gives the empirical formula, see table 1.

3.2. *UV-visible spectra*

UV-vis spectral data of ligands and complexes are given in table 2. Characteristic Q and B (Soret) bands of porphyrins and metal porphyrins complexes in visible and near UV ranges are assigned to the transitions from ground state (S_0) to the lowest excited singlet (S_1) and second lowest excited singlet state (S_2), respectively. The absorption spectra of all the complexes are very similar. Compared with the ligands, the number of absorption bands of the complexes has decreased, which is attributed to the increased symmetry of the complexes. Soret bands shift slightly to longer wavelengths. These results are in accord with those in the literature [14, 15].

3.3. *Molar conductances*

The molar conductance values of the ligand H_2[(C_{12}OEOP)$_4$P] and its complexes with Yb(III), Er(III), Dy(III), Tb(III) are 0.126, 0.165, 0.180, 0.145, 0.160, respectively. Those of the ligand H_2[(C_{14}OEOP)$_4$P] and the corresponding complexes are 0.121, 0.045, 0.157, 0.170, 0.160, respectively. Those of the ligand H_2[(C_{16}OEOP)$_4$P] and the corresponding complexes are 0.148, 0.170, 0.155, 0.153, 0.195, respectively. All the data indicate that the ligands and all the complexes show non-electrolytic behaviour [16].

3.4. *Infrared spectra*

The main spectral band frequencies of the ligands and complexes are listed in table 3 [17, 18]. The spectral

Table 1. Characterization data of the compounds[a].

Compound	Empirical formula	C/%	H/%	N/%	Yield/%	Dec.temp./°C
$H_2[(C_{12}OEOP)_4P]$	$C_{100}N_4O_8H_{142}$	78.60 (78.63)	9.31 (9.30)	3.66 (3.67)	75	>400
$H_2[(C_{14}OEOP)_4P]$	$C_{108}N_4O_8H_{158}$	79.15 (79.12)	9.61 (9.64)	3.40 (3.41)	73	>400
$H_2[(C_{16}OEOP)_4P]$	$C_{116}N_4O_8H_{174}$	79.56 (79.54)	9.45 (9.44)	3.21 (3.20)	75	>400
$Yb[(C_{12}OEOP)_4P(OH)]$	$YbC_{100}N_4O_9H_{141}$	69.65 (69.68)	8.28 (8.28)	3.25 (3.26)	85	>200
$Er[(C_{12}OEOP)_4P(OH)]$	$ErC_{100}N_4O_9H_{141}$	70.25 (70.22)	8.34 (8.31)	3.26 (3.27)	88	>200
$Dy[(C_{12}OEOP)_4P(OH)]$	$DyC_{100}N_4O_9H_{141}$	70.45 (70.41)	8.30 (8.33)	3.27 (3.28)	83	>200
$Tb[(C_{12}OEOP)_4P(OH)]$	$TbC_{100}N_4O_9H_{141}$	70.59 (70.56)	8.32 (8.35)	3.30 (3.29)	85	>200
$Yb[(C_{14}OEOP)_4P(OH)]$	$YbC_{108}N_4O_9H_{157}$	70.90 (70.94)	8.63 (8.65)	3.05 (3.06)	86	>200
$Er[(C_{14}OEOP)_4P(OH)]$	$ErC_{108}N_4O_9H_{157}$	71.12 (71.17)	8.69 (8.68)	3.06 (3.07)	88	>200
$Dy[(C_{14}OEOP)_4P(OH)]$	$DyC_{108}N_4O_9H_{157}$	71.36 (71.35)	8.68 (8.70)	3.07 (3.08)	80	>200
$Tb[(C_{14}OEOP)_4P(OH)]$	$TbC_{108}N_4O_9H_{157}$	71.45 (71.49)	8.70 (8.72)	3.07 (3.08)	88	>200
$Yb[(C_{16}OEOP)_4P(OH)]$	$YbC_{116}N_4O_9H_{173}$	71.75 (71.79)	8.98 (9.01)	2.89 (2.89)	86	>200
$Er[(C_{16}OEOP)_4P(OH)]$	$ErC_{116}N_4O_9H_{173}$	72.03 (72.00)	9.89 (9.01)	2.88 (2.89)	86	>200
$Dy[(C_{16}OEOP)_4P(OH)]$	$DyC_{116}N_4O_9H_{173}$	72.14 (72.18)	9.00 (9.03)	2.89 (2.90)	80	>200
$Tb[(C_{16}OEOP)_4P(OH)]$	$TbC_{116}N_4O_9H_{173}$	72.30 (72.32)	9.02 (9.05)	2.89 (2.90)	80	>200

[a]Theoretical values in parenthesis.

bands at 971 and 3313 cm^{-1} in the ligand porphyrin are assigned to the N–H bending and stretching vibrations of the porphyrin core. These two vibration bands disappear in the complexes since the hydrogen atoms of the porphyrin core are replaced by the lanthanide ion to form a Ln–N bond. The –C=N stretching vibration of the pyrrole ring for the ligand is at 1345 cm^{-1}, and this band in the complexes shifts to lower wavenumbers, 1333–1334 cm^{-1}, providing clear evidence that the nitrogen atoms of the porphyrin core are coordinated to the lanthanide ion. The existence of the Ln–OH bending vibration band in the region 1067–1079 cm^{-1} shows that the oxygen atom of the hydroxy group is bound to the lanthanide ion. Assignments of other absorption bands are also given in table 3.

3.5. *^{1}H NMR spectra*

The ^{1}H NMR chemical shift values in deuterated chloroform (δ,ppm) for the ligands and complexes are collected in table 4. Compared with the ligand, the signal at −2.76 ppm for the complex $Tb[(C_{14}OEOP)_4P(OH)$ disappears, since the hydrogen atom in the N–H bond is replaced by the lanthanide ion, and the signal at 0.39 ppm appears, the latter being due to hydroxy oxygen coordinated to the lanthanide ion. The disappearance of the signal at −2.76 ppm and the appearance of the signal at 0.39 ppm indicate that the porphyrin ligand and hydroxy group are coordinated to the lanthanide ion.

3.6. *Differential scanning calorimetry*

The transition temperatures and associated enthalpy changes of the various porphyrin ligands and complexes are given in table 5. The DSC data of the complexes are summarized in figure 1. The numbers of liquid crystal phases of the ligands with twelve, fourteen and sixteen carbons are one, two and three, respectively, revealing enhanced polymorphism on increasing chain length. The transition temperatures for the first liquid crystal phase of the complexes tend to room temperature on increasing the chain length, and we expect that they may be used as liquid crystal materials in the future. The optical textures of the free base and the complexes are given in figure 2.

Table 2. UV-vis spectral data of ligands and complexes.[a]

Compound	λ_{max}/nm				
	B band (Soret)	Q band			
$H_2[(C_{12}OEOP)_4P]$	426 (2.5×10^5)	520 (1.1×10^4)	558 (7.5×10^3)	595 (3.7×10^3)	651 (4.3×10^3)
$H_2[(C_{14}OEOP)_4P]$	426 (2.1×10^5)	520 (8.1×10^3)	559 (5.0×10^3)	592 (2.1×10^3)	651 (2.7×10^3)
$H_2[(C_{16}OEOP)_4P]$	426 (9.2×10^4)	521 (4.0×10^3)	559 (2.7×10^3)	592 (2.0×10^3)	651 (1.7×10^3)
$Yb[(C_{12}OEOP)_4P(OH)]$	428 (2.3×10^5)	519 (4.6×10^3)	554 (1.0×10^5)	594 (3.6×10^4)	
$Er[(C_{12}OEOP)_4P(OH)]$	429 (1.9×10^5)	519 (4.5×10^3)	556 (8.1×10^4)	597 (3.2×10^4)	
$Dy[(C_{12}OEOP)_4P(OH)]$	430 (1.2×10^5)	519 (1.7×10^4)	559 (7.4×10^4)	601 (3.5×10^4)	
$Tb[(C_{12}OEOP)_4P(OH)]$	430 (1.5×10^5)	518 (2.1×10^4)	557 (6.5×10^4)	596 (2.6×10^4)	
$Yb[(C_{14}OEOP)_4P(OH)]$	428 (2.2×10^5)	517 (2.9×10^4)	554 (1.3×10^5)	594 (4.6×10^4)	
$Er[(C_{14}OEOP)_4P(OH)]$	429 (2.3×10^5)	518 (2.8×10^4)	555 (1.2×10^5)	594 (4.3×10^4)	
$Dy[(C_{14}OEOP)_4P(OH)]$	430 (1.8×10^5)	518 (9.3×10^3)	556 (7.9×10^4)	595 (2.9×10^4)	
$Tb[(C_{14}OEOP)_4P(OH)]$	430 (2.0×10^5)	519 (2.4×10^4)	556 (8.9×10^4)	596 (3.3×10^4)	
$Yb[(C_{16}OEOP)_4P(OH)]$	429 (1.9×10^5)	519 (2.4×10^3)	554 (1.5×10^4)	594 (7.8×10^3)	
$Er[(C_{16}OEOP)_4P(OH)]$	429 (1.1×10^5)	519 (1.3×10^4)	554 (4.9×10^4)	594 (1.9×10^4)	
$Dy[(C_{16}OEOP)_4P(OH)]$	428 (3.2×10^5)	519 (7.2×10^3)	556 (4.8×10^4)	595 (1.8×10^4)	
$Tb[(C_{16}OEOP)_4P(OH)]$	430 (2.4×10^5)	519 (4.9×10^3)	556 (1.8×10^4)	595 (9.3×10^3)	

[a]Molar extinction coefficient in parenthesis.

Table 3. Infrared spectral frequencies (cm^{-1}) of the ligands and complexes: m=medium, w=weak.

Compound	O–H Str.	N–H Str. (Pyrrole)	C–C Str. (Benzol)	C–H Bend (Pyrrole)	Ln–OH Bend	–C=N Str. (Pyrrole)	C–O–C Bend (Ethoxyl)	N–H Bend (Pyrrole)
$H_2[(C_{12}OEOP)_4P]$		3313w	1591m	1466m		1345w	1248m	971m
$H_2[(C_{14}OEOP)_4P]$		3313w	1598m	1466m		1345w	1248m	971m
$H_2[(C_{16}OEOP)_4P]$		3313w	1586m	1466m		1345w	1248m	971m
$Yb[(C_{12}OEOP)_4P(OH)]$	3420m		1574m	1466m	1067m	1333w	1250m	
$Er[(C_{12}OEOP)_4P(OH)]$	3422m		1574m	1466m	1067m	1333w	1248m	
$Dy[(C_{12}OEOP)_4P(OH)]$	3422m		1575w	1466m	1079m	1333w	1248m	
$Tb[(C_{12}OEOP)_4P(OH)]$	3423m		1565w	1466m	1067m	1333w	1252m	
$Yb[(C_{14}OEOP)_4P(OH)]$	3434m		1598w	1466m	1067m	1333w	1250m	
$Er[(C_{14}OEOP)_4P(OH)]$	3434m		1598w	1466m	1079m	1334w	1256m	
$Dy[(C_{14}OEOP)_4P(OH)]$	3410m		1600w	1466w	1079m	1333w	1260m	
$Tb[(C_{14}OEOP)_4P(OH)]$	3428m		1598w	1466w	1067m	1333w	1250m	
$Yb[(C_{16}OEOP)_4P(OH)]$	3410m		1574w	1466m	1067m	1333w	1260m	
$Yb[(C_{16}OEOP)_4P(OH)]$	3422m		1600w	1466m	1079m	1333w	1248m	
$Dy[(C_{16}OEOP)_4P(OH)]$	3420m		1586w	1466m	1079m	1333w	1256m	
$Tb[(C_{16}OEOP)_4P(OH)]$	3410m		1574w	1466m	1067m	1333w	1246m	

Table 4. ^{1}H NMR spectral bands of ligands and complexes.

Compound	Proton number	Proton position	δ/ppm
$H_2[(C_{14}OEOP)_4P]$	8H	pyrrole, ring	8.90
	12H	meso-phenyl protons	7.78,7.71
	16H	C_6H_4–O–CH_2 protons	4.20
	24H	–CH_3	0.88
	96H	–$(CH_2)_{12}$–	1.64, 1.26,1.38, 1.49
	2H	pyrrole N–H	−2.76
$Tb[(C_{14}OEOP)_4P(OH)]$	8H	pyrrole, ring	8.75
	12H	meso-phenyl protons	7.47
	16H	C_6H_4–O–CH_2 protons	4.07
	24H	–CH_3	0.74
	96H	–$(CH_2)_{12}$–	1.10
	1H	–OH	0.39

Table 5. Phase transition temperatures and enthalpy changes of the porphyrin compounds on heating at 10°C min^{-1}.

Compound	T/°C (ΔH/kJ mol^{-1})				
$H_2[(C_{12}OEOP)_4P]$	C_r −53.5(1.4)	LC 64.4(30.9)			I
$H_2[(C_{14}OEOP)_4P]$	C_r 6.7(20.6)	LC_1 36.1(0.4)	LC_2 69.6(48.8)		I
$H_2[(C_{16}OEOP)_4P]$	C_r −0.3(2.1)	LC_1 22.2(19.0)	LC_2 37.2(36.8)	LC_3 65.6(45.7)	I
$Yb[(C_{12}OEOP)_4P(OH)]$	C_r −33.8(0.2)	LC 71.9(48.6)			I
$Er[(C_{12}OEOP)_4P(OH)]$	C_r −43.7(5.4)	LC 101.0(4.8)			I
$Dy[(C_{12}OEOP)_4P(OH)]$	C_r 8.5(0.1)	LC 15.4(4.4)			I
$Tb[(C_{12}OEOP)_4P(OH)]$	C_r −32.8(39.3)	LC 6.9(1.5)			I
$Yb[(C_{14}OEOP)_4P(OH)]$	C_r −4.1(50.7)	LC_1 37.0(1.4)	LC_2 43.6(3.8)		I
$Er[(C_{14}OEOP)_4P(OH)]$	C_r −3.5(54.3)	LC_1 29.9(4.0)	LC_2 50.3(10.3)		I
$Tb[(C_{14}OEOP)_4P(OH)]$	C_r −2.8(50.2)	LC 49.5(12.5)			I
$Yb[(C_{16}OEOP)_4P(OH)]$	C_r 32.0(0.1)	LC 66.4(0.7)			I
$Er[(C_{16}OEOP)_4P(OH)]$	C_r −0.1(0.9)	LC 21.0(5.9)			I
$Dy[(C_{16}OEOP)_4P(OH)]$	C_r 0.2(2.3)	LC 15.1(20.8)			I
$Tb[(C_{16}OEOP)_4P(OH)]$	C_r 19.0(10.1)	LC_1 30.9(14.9)	LC_2 69.7(1.4)		I

3.7. *X-ray diffraction*

Small angle XRD of the complexes at room temperature revealed reflections with *d*-spacing (listed in table 6), which correspond to the first three reflections of a hexagonal columnar structure (reciprocal *d*-spacing of 1:1/$\sqrt{3}$:1/2). Figure 3 gives the XRD trace of $Dy[(C_{16}OEOP)_4P(OH)]$. The mesophase structure is proposed to be a hexagonal columnar, Col_h. Wide angle XRD shows only a broad halo (centered at $2\theta=20^\circ$), which arises from the molten alkyl chains.

3.8. *Luminescence of the ligands and complexes*

Tables 7 and 8 give the excitation and emission spectral data of the ligands and complexes, respectively. The emission spectra and excitation spectra of ligand $H_2[(C_{12}OEOP)_4P]$ and complex $Tb[(C_{12}OEOP)_4P(OH)]$ are shown in figures 4 and 5, respectively.

Soret bands of all the ligands and five of the complexes split into two bands, comparing the UV-vis absorption spectra, while the near 651 nm bands of three ligands disappear. Other spectral bands undergo only a small change. Fluorescence of the S_2 (B, Soret band) and S_1(Q band) are observed in the porphyrin complexes, of which the B (Soret) band is attributed to transition from the second excited singlet state S_2 to ground state S_0, $S_2 \rightarrow S_0$. The Soret fluorescence is about two orders of magnitude weaker than the $S_1 \rightarrow S_0$ of Q band emission. Its quantum yield is so low that sometimes fluouescence becomes unobservable. This fluorescence emission does not occur at room temperature in our experimental excited wavelength, 420 nm. Q(0–0) fluorescence bands of the complexes are in the region 598–619 nm, and only seven complexes have Q(0–0) bands. Q(0–1) fluorescence bands of the complexes are in the region 656–661 nm, and Q(0–2) bands at 720–730 nm. They show mirror symmetry with the

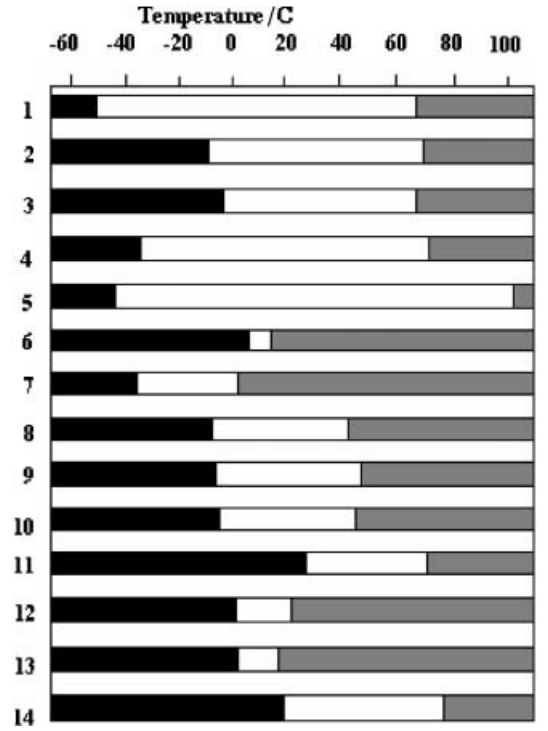

Figure 1. The transition temperatures of $H_2[(C_nOEOP)_4P]$ (1, 2, 3 correspond to n=12, 14, 16, respectively) and $Ln[(C_nOEOP)_4P(OH)]$ (4, 5, 6, 7 correspond to n=12, Ln=Yb, Er, Dy, Tb; 8, 9, 10 correspond to n=14, Ln=Yb, Er, Tb; 11, 12, 13, 14 correspond to n=16, Ln=Yb, Er, Dy, Tb, respectively), showing the temperature ranges of crystalline phase (black), liquid crystal phase (white), and isotropic phase (grey).

absorption spectra. The quantum yields (Φ_f) of the Q band for the complexes are in the range 0.0014–0.038, and for the ligands 0.084–0.1145. The $S_1 \rightarrow S_0$ quantum yield depends on the relative rates of the radiative process $S_1 \rightarrow S_0$ and the two radiationless processes $S_1 \rightsquigarrow S_0$ and $S_1 \rightsquigarrow Tn$. The quantum yields of the complexes are lower than those of the ligands. The fluorescence quantum yields of our complexes are much lower than 0.20. Thus, the excited state of the complexes S_1 is primarily deactivated by radiationless decay. Therefore, the spin-forbidden process $S_1 \rightsquigarrow Tn$ is the predominant route for radiationless deactivation of S_1 in the complexes.

These quantum yields (Φ_f) were calculated using the equation:

$$\Phi_f = \Phi_{fs} n^2 A_s I_f / \left(n_s^2 A I_{fs}\right)$$

where n_s, A_s and I_{fs} are the refractive index, absorbance and integrated intensity of a standard sample at the excited wavelength, respectively. Meso-tetraphenylporphyrin zinc, ZnTPP, was used as the standard sample, Φ_{fs}=0.033 [19].

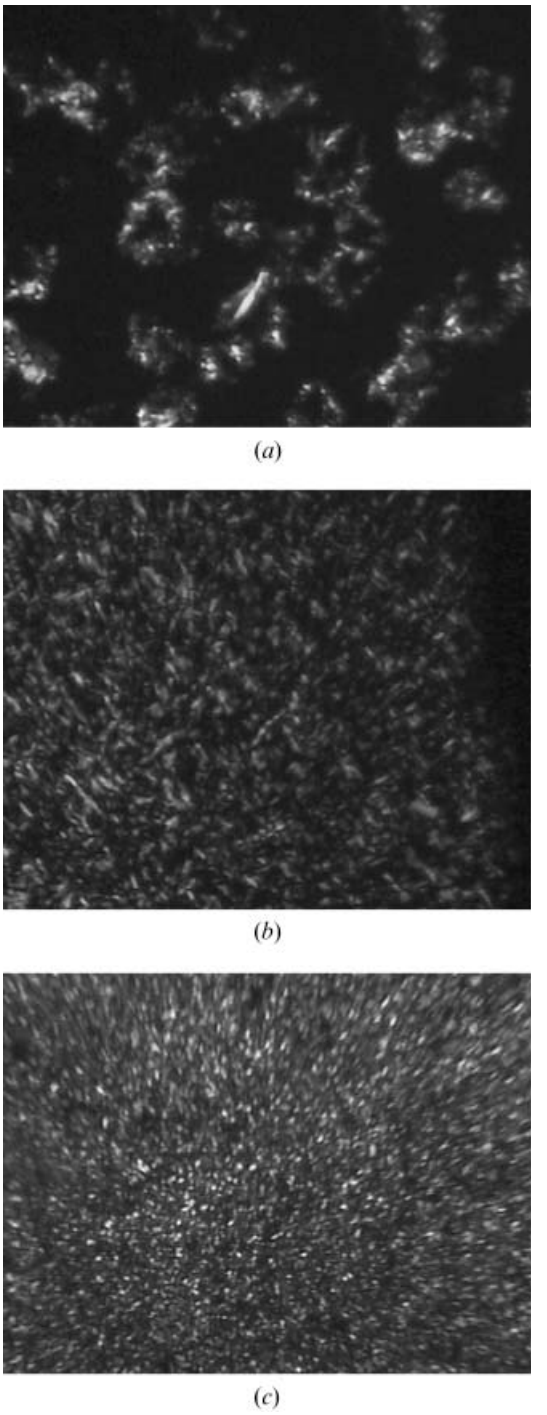

(a)

(b)

(c)

Figure 2. Optical textures of (*a*) $H_2[(C_{16}OEOP)_4P]$ at 6°C, (*b*) $Tb[(C_{14}OEOP)_4P(OH)]$ at −2.9°C and (*c*) $Tb[(C_{16}OEOP)_4P(OH)]$ at 16.7°C.

3.9. *Thermal stability of the ligands and complexes*

Figure 6 gives the DTA and TGA curves of the ligand $H_2[(C_{12}OEOP)_4P]$ and complex $Dy[(C_{16}OEOP)_4P(OH)]$. The thermal analytical data of selected ligands and

Table 6. Room temperature XRD data of four complexes.

Compound	Spacing/Å	Miller indices
Er[$(C_{12}OEOP)_4P(OH)$]	28.0, 16.8, 14.1	100, 110, 200
Er[$(C_{14}OEOP)_4P(OH)$]	29.8, 17.7, 15.0	100, 110, 200
Yb[$(C_{14}OEOP)_4P(OH)$]	28.1, 16.8, 14.1	100, 110, 200
Dy[$(C_{16}OEOP)_4P(OH)$]	31.7, 19.1, 16.0	100, 110, 200

Table 7. Excitation spectral data of ligands and complexes.

Compound	Peak values/nm				
$H_2[(C_{12}OEOP)_4P]$	411	437	521	556	594
$H_2[(C_{14}OEOP)_4P]$	418	434	520	555	593
$H_2[(C_{16}OEOP)_4P]$	419	431	520	556	594
Yb[$(C_{12}OEOP)_4P(OH)$]	418	436	522	556	601
Er[$(C_{12}OEOP)_4P(OH)$]	418	434	519	556	597
Dy[$(C_{12}OEOP)_4P(OH)$]	419		521	556	592
Tb[$(C_{12}OEOP)_4P(OH)$]	422		520	559	594
Yb[$(C_{14}OEOP)_4P(OH)$]	416	435	520	558	590
Er[$(C_{14}OEOP)_4P(OH)$]	419	434	518	552	598
Dy[$(C_{14}OEOP)_4P(OH)$]	419		517	553	593
Tb[$(C_{14}OEOP)_4P(OH)$]	418	434	520	552	598
Yb[$(C_{16}OEOP)_4P(OH)$]	427		522	557	590
Er[$(C_{16}OEOP)_4P(OH)$]	419		520	559	604
Dy[$(C_{16}OEOP)_4P(OH)$]	419		520	558	591
Tb[$(C_{16}OEOP)_4P(OH)$]	424		518	557	590

Table 8. Emission spectral data of ligands and complexes.

	Peak value/nm			
Compound	Q(0–0)	Q(0–1)	Q(0–2)	Quantum yield, Φ_f
$H_2[(C_{12}OEOP)_4P]$		656	726	0.08411
$H_2[(C_{14}OEOP)_4P]$		659	722	0.1125
$H_2[(C_{16}OEOP)_4P]$		658	727	0.1145
Yb[$(C_{12}OEOP)_4P(OH)$]	606	661	723	0.001411
Er[$(C_{12}OEOP)_4P(OH)$]	603	658	721	0.002634
Dy[$(C_{12}OEOP)_4P(OH)$]	609	656	720	0.008785
Tb[$(C_{12}OEOP)_4P(OH)$]		659	720	0.02914
Yb[$(C_{14}OEOP)_4P(OH)$]	619	658	726	0.003843
Er[$(C_{14}OEOP)_4P(OH)$]	598	657	722	0.004480
Dy[$(C_{14}OEOP)_4P(OH)$]		657	727	0.01022
Tb[$(C_{14}OEOP)_4P(OH)$]		656	727	0.01794
Yb[$(C_{16}OEOP)_4P(OH)$]		657	730	0.004370
Er[$(C_{16}OEOP)_4P(OH)$]	603	660	720	0.009538
Dy[$(C_{16}OEOP)_4P(OH)$]	608	657	725	0.006149
Tb[$(C_{16}OEOP)_4P(OH)$]		657	725	0.03864

Table 9. Thermal analytical data of selected ligands and complexes.

Compound	Decomposition region/°C	Exothermal peaks/°C	Final weight/%
$H_2[(C_{12}OEOP)_4P]$	400–900	675,721,869	0
$H_2[(C_{14}OEOP)_4P]$	405–900	673,708,850	0
$H_2[(C_{16}OEOP)_4P]$	420–900	670,810,890	0
Er[$(C_{12}OEOP)_4P(OH)$]	198–800	387,415,508	11
Er[$(C_{14}OEOP)_4P(OH)$]	200–800	370,520,570	10
Dy[$(C_{16}OEOP)_4P(OH)$]	196–800	362,446,499	9

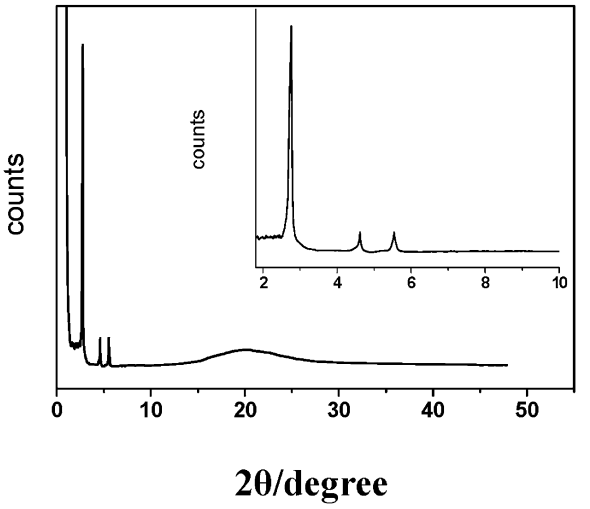

Figure 3. X-ray diffraction patterns of Dy[$(C_{16}OEOP)_4$ P(OH)] at room temperature.

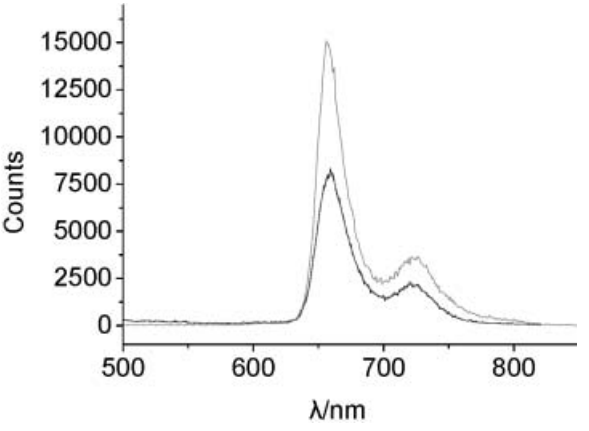

Figure 4. Emission spectra of ligand. $H_2[(C_{12}OEOP)_4P]$ (……); complex Tb[$(C_{12}OEOP)_4P(OH)$](—).

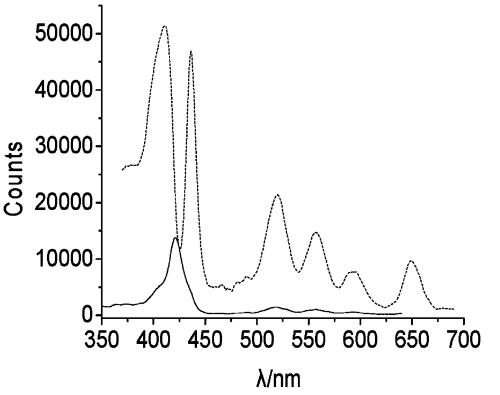

Figure 5. Excitation spectra of ligand. $H_2[(C_{12}OEOP)_4P]$ (……); complex Tb[$(C_{12}OEOP)_4P(OH)$](—).

complexes are listed in table 9. Thermal analysis shows that the complexes are stable in the region 196–200°C. The TGA and DTA curves do not contain steps or peaks in the region 196–200°C; therefore the complexes do not contain small molecules (water or solvent). The complexes undergo complete decomposition up to 800°C, with a residue of 9–11% rare earth oxide Ln_2O_3. The ligands are stable in the region 400–420°C. The onset and upper decomposition temperatures of the ligands are all higher than those of the complexes, which indicates that the stability of the ligands is higher than that of the complexes.

3.10. *Cyclic voltammetry*

Cyclic voltammetric studies have been performed to evaluate the redox potentials and to determine the HOMO-LUMO energy level. The porphyrin ring has higher HOMO($3a_{2u}(\pi)$) and lower LUMO($4e_g(\pi^*)$). It should undergo oxidation reactions in HOMO and reduction reactions in LUMO

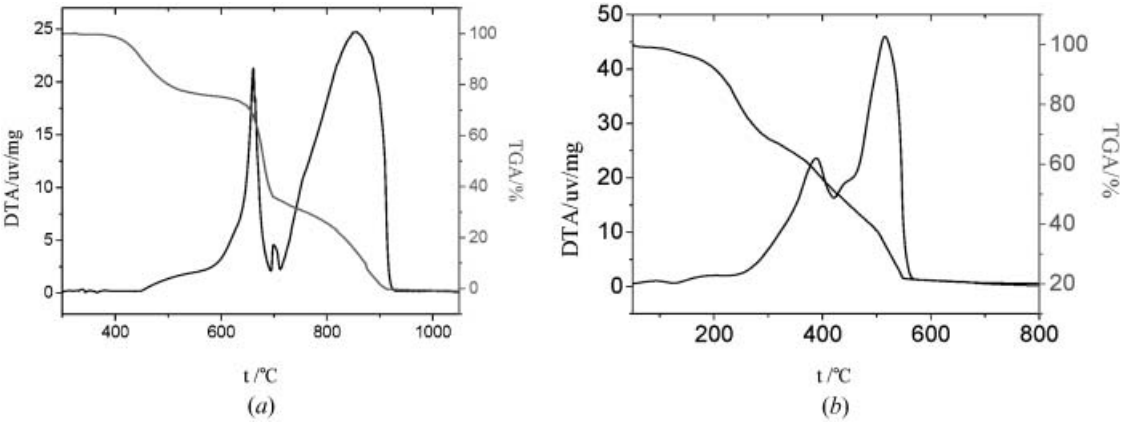

Figure 6. TGA and DTA traces (*a*) of ligand $H_2[(C_{12}OEOP)_4P]$ and (*b*) complex Er[$(C_{12}OEOP)_4P(OH)$].

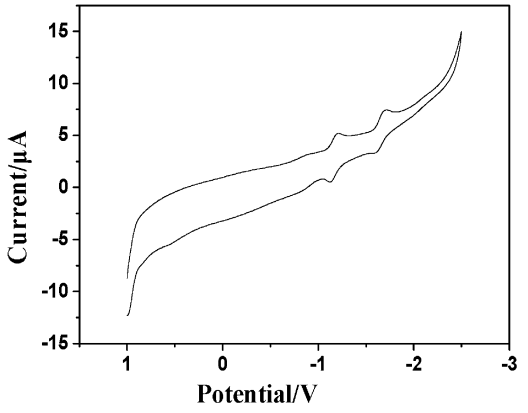

Figure 7. Cyclic voltammogram of $H_2[(C_{14}OEOP)_4P]$(DMF, room temperature, $[Bu_4N][ClO_4]$ as supporting electrolyte, Ag/Ag^+ electrode).

levels. In the cyclic voltammograms of $H_2[(C_{12}OEOP)_4P]$, $H_2[(C_{14}OEOP)_4P]$, $H_2[(C_{16}OEOP)_4P]$ and $Er[(C_{14}OEOP)_4P(OH)]$ in 0.1M tetrabutylammonium perchlorate in DMF, within the accessible potential window of the solvent, two quasi-reversible couples of the three ligands and three quasi-reversible couples of $Er[(C_{14}OEOP)_4P(OH)]$ were observed. The first and second one-electron redox potentials corresponding to the porphyrin ring reaction of $H_2[(C_{12}OEOP)_4P]$, $H_2[(C_{14}OEOP)_4P]$ and $H_2[(C_{16}OEOP)_4P]$ are located at $E_{1/2}=-1.170$, -1.664; -1.173, -1.678 and -1.168, -1.646 V vs Ag/Ag^+, respectively. The corresponding potentials for the porphyrin ring reaction of $Er[(C_{14}OEOP)_4P(OH)]$ (referred to as $Er^{III}POH$ for brevity) are located at -1.405 and -1.611 V vs Ag/Ag^+, which produce the π anions $(Er^{III}POH)^-$ and $(Er^{III}POH)^{2-}$, respectively. The third quasi-reversible reduction of $Er^{III}POH$ concerning the lanthanide metal (erbium) ion is located at -2.018 V vs Ag/Ag^+ and generates an erbium(II) porphyrin anion $(Er^{II}P)^-$. These essential processes are characterized by the equation:

$$Er^{III}POH + e^- \rightarrow (Er^{III}POH)^- + e^-$$
$$\rightarrow (Er^{III}POH)^{2-} + e^- \rightarrow (Er^{II}POH)^{3-}.$$

Figure 7 gives the voltammograms of $H_2[(C_{14}OEOP)_4P]$. It is found that the two redox steps of the ligands are at very close potentials. The similarity of the redox potentials implies that they do not change on varying the chain length (n=12, 14, 16).

4. Conclusion

In a lanthanide porphyrin complex, one molecular porphyrin ligand is coordinated to a lanthanide ion in a tetradentate fashion, and a hydroxyl group is coordinated to the same lanthanide ion. Therefore, the coordination number of the central rare earth ion is five [20, 21] and the general formula of the complexes may be represented as $Ln[(C_nOEOP)_4P(OH)]$ (n=12, 14, 16). The rare earth ion is expected to lie above the porphyrin molecular plane (see figure 8). The mesophase structure is a hexagonal columnar phase.

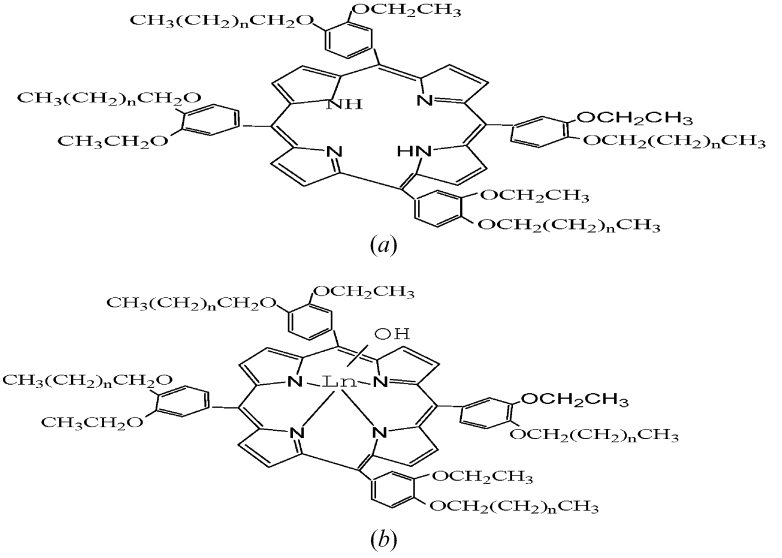

Figure 8. The structures of (*a*) the ligand $H_2[(C_nOEOP)_4P]$ (n=12, 14, 16), and (*b*) complex $Ln[(C_nOEOP)_4P(OH)]$(n=12, 14, 16; Ln=Yb, Er, Dy, Tb).

Acknowledgement

We thank the National Natural Science Foundation of China for financial support of this work.

References

[1] C.P. Wong, R.F. Ventelcher, W.D. Horrocks, Jr., *J. Am. chem. Soc.*, **96**, 7149 (1974).
[2] D. Dorphin. *The Porphyrins*, Vols. I–VII, Academic Press, New York (1978).
[3] G.W. Gray, P.A. Winsor. *Liquid Crystals and Plastic Crystals*, Vols. I and II, Wiley, New York (1974).
[4] G.H. Brown (Ed.). *Advances in Liquid Crystals*, Vols. 1–6, Academic Press, New York (1975–1983).
[5] S. Chandrasckhar, B.K. Sadashiva, K.A. Suresl. *Pramana*, **9**, 471 (1977).
[6] J.W. Goodby, P.S. Robinson, B.K. Teo, P.E. Cladis. *Mol. Cryst. liq. Cryst. Lett.*, **56**, 303 (1980).
[7] Y. Shimizu, M. Miya. *Chem. Lett.*, p. 25 (1991).
[8] R. Ramasseul, P. Maldivi, J.C. Marchon, M. Taylor, D. Guillon. *Liq. Cryst.*, **13**, 729 (1993).
[9] S. Chandrasekhar. *Liq. Cryst.*, **14**, 3 (1993).
[10] C.-Y. Liu, H.-L. Pan, M.A. Fox, A.J. Bard. *Science*, **261**, 897 (1993).
[11] W. Liu, Y.H. Shi, T.S. Shi, G.F. Liu, Y.X. Liu, C. Wang, W.J. Zhang. *Liq. Cryst.*, **30**, 1255 (2003).
[12] W.D. Horrocks, M. Albin. *Progress in Inorganic Chemistry*, Vol. 31, S.J. Lippard (Ed.), p. 1104, Wiley (1984).
[13] T.S. Shi, W. Liu, G.F. Liu. *Chin. J. apll. Chem.*, **15**, 75 (1998).
[14] G.F. Liu, T.S. Shi. *Synth. React. inorg. met.-org. Chem.*, **23**, 1145 (1993).
[15] G.F. Liu, T.S. Shi. *Synth. React. inorg. met.-org. Chem.*, **24**, 1127 (1994).
[16] C.P. Wong, W.D. Jr. Horrocks. *Tetrahedron Lett.*, 2637 (1975).
[17] G.F. Liu, T.S. Shi. *Polyhedron*, **13**, 2255 (1994).
[18] G.F. Liu, Y.F. Zhang. *Chem. J. Chin. Univ.*, **5**, 713 (1984).
[19] D.J. Quimby, F.R. Longo. *J. Am. chem. Soc.*, **77**, 5111 (1975).
[20] W.D. Horrocks, Jr., E.G. Hove. *J. Am. chem. Soc.*, **100**, 4386 (1978).
[21] M. Gouterman, C.P. Schumaker, T.S. Srivastava, T. Yonetani. *Chem. Phys. Lett.*, **40**, 456 (1976).